Evaluation of IL-1 blockade as a host-directed therapy for tuberculosis in mice and macaques

Caylin G. Winchell[1], Bibhuti B. Mishra [2,3], Jia Yao Phuah[2], Mohd Saqib[3], Samantha J. Nelson[2], Pauline Maiello[1], Chelsea M. Causgrove[1], Cassaundra L. Ameel[1], Brianne Stein[1], H. Jacob Borish[1], Alexander G. White[1], Edwin C. Klein[4], Matthew D. Zimmerman[5¥], Véronique Dartois[5¥], Philana Ling Lin[6], Christopher M. Sassetti[2], JoAnne L. Flynn[1*]

[1]Department of Microbiology and Molecular Genetics, University of Pittsburgh School of Medicine, Pittsburgh, Pennsylvania, USA

[2]Department of Microbiology and Physiological Systems, University of Massachusetts Medical School, Worcester, Massachusetts, USA

[3]Department of Immunology and Microbial Disease, Albany Medical College, Albany, New York, USA

[4]Division of Laboratory Animal Research, University of Pittsburgh, Pittsburgh Pennsylvania, USA

[5]Public Health Research Institute, New Jersey Medical School, Rutgers, The State University of New Jersey, Newark, NJ, USA

[6]Department of Pediatrics, UPMC Children's Hospital of the University of Pittsburgh, Pittsburgh, Pennsylvania, USA

¥ Present address: Center for Discovery and Innovation, Hackensack Meridian Health, Nutley, NJ, USA

* Corresponding author

Email: joanne@pitt.edu

Abstract

In 2017, there were over 550,000 estimated new cases of multi-drug/rifampicin resistant tuberculosis (MDR/RR-TB), emphasizing a need for new treatment strategies. Linezolid (LZD) is a potent antibiotic for antibiotic-resistant Gram-positive infections and is an effective treatment for TB. However, extended LZD use can lead to LZD-associated host toxicities, most commonly bone marrow suppression. LZD toxicities may be mediated by IL-1, a pathway important for early immunity during *M. tuberculosis* infection that later contributes to pathology. We hypothesized LZD efficacy could be enhanced by modulation of IL-1 pathway to reduce BM toxicity and TB associated-inflammation. We used two animal models of TB to test our hypothesis, mice and cynomolgus macaques. Antagonizing IL-1 in chronically-infected mice reduced lung neutrophil numbers and partially restored the erythroid progenitor populations that are depleted by LZD. In macaques, we found no conclusive evidence of BM suppression associated with LZD, indicating our treatment time may have been short enough to avoid the toxicities observed in humans. Though treatment was only 1 month, the majority of granulomas were sterilized with reduced inflammation (assessed by PET/CT) in animals treated with both LZD and IL-1 receptor antagonist (IL-1Rn). However, overall lung inflammation was significantly reduced in macaques treated with both IL-1Rn and LZD, compared to LZD alone. Importantly, IL-1Rn administration did not noticeably impair the host response against Mtb or LZD efficacy in either animal model. Together, our data support that inhibition of IL-1 in combination with LZD has potential to be an effective HDT for TB.

Author summary

Host-directed therapies (HDTs) are a potential option in combating drug resistant TB as they can circumvent bacterial drug-resistance by targeting host responses rather than the pathogen. Here we designed an HDT to target the IL-1 pathway, an inflammatory immune

response that is both critical and detrimental to TB disease outcome. We combined IL-1Rn, an IL-1R antagonist, with linezolid (LZD) which is an effective antibiotic for drug-resistant M. tuberculosis. Extended treatment causes severe host-toxicities that might be mediated in part by the IL-1 pathway. Our goals were to enhance LZD efficacy by negating LZD-host toxicities and to reduce adverse inflammation caused by TB. In mice, IL-1Rn effectively reduced inflammatory signatures associated with TB and reversed linezolid-induced bone marrow suppression, the most common toxicity. In cynomolgus macaques, inflammation, as assessed by PET/CT, was reduced by the combination of IL-1Rn and LZD therapy, compared to LZD alone. In contrast to mice, we did not observe bone marrow suppression in macaques, highlighting the importance of both models when assessing prospective therapies. These data show the potential of IL-1Rn as a therapy for TB and support LZD as an effective antibiotic against drug-resistant TB.

Introduction

Tuberculosis (TB) remains the top cause of death by a single infectious agent, with an estimated 10 million new active TB cases and 1.3 million deaths in 2017 alone (1). Antibiotic treatment regimens are long and multi-drug resistant (MDR) and extensive-drug resistant (XDR) *Mycobacterium tuberculosis* (Mtb) strains have emerged, complicating treatment. Even those patients that are cured of the infection can suffer permanent deficits in lung function that result from inflammation and fibrosis (2). Host-directed therapies (HDTs) have been proposed as a potential option for improving therapy. Depending on the strategy, HDTs could enhance antimicrobial immune responses and shorten therapy, or inhibit pathological inflammation (3). Since HDT would be used as part of a multi-drug regimen, targeting mechanisms that increase drug exposure or decrease toxicity could also be envisioned. While some HDT strategies hold promise, very few have been rigorously tested in pre-clinical models (4).

Interleukin-1 (IL-1) has been implicated in TB disease and inflammation, making it a possible target of HDT. This cytokine plays an important yet complicated role in TB disease progression. The susceptibility of mice lacking critical mediators of IL-1 signaling indicates that some initial production of IL-1β upon Mtb infection is essential for priming downstream immune responses necessary for disease control (5-8). In contrast, IL-1 is also responsible for the accumulation of disease-promoting neutrophils in chronically-infected susceptible mice, and genetic variants that result in higher IL-1β production are associated with increased disease severity and neutrophil accumulation in humans (9-11). Given that HDT is designed to be administered to chronically-infected patients during treatment, when persistent IL-1 production appears to play a more pathological role, it could be beneficial to block the inflammation and disease promoting activities of this cytokine.

IL-1 may also play a role in the toxicity of linezolid (LZD), an increasingly important antibiotic for the treatment of drug-resistant TB, highlighted by its recent inclusion in a newly approved therapy for MDR-TB (12). While LZD has shown efficacy against XDR and MDR TB, its wide-spread use has been limited by severe host toxicities that occur after more than 4 weeks of treatment (13, 14). Over the 6-20 month treatment course necessary to treat resistant TB, both reversible bone marrow suppression and irreversible neuropathies are common (15). LZD-associated toxicities are generally attributed to the inhibition of mitochondrial translation and LZD-mediated bone marrow suppression is promoted by the subsequent mitochondrial damage. This damage acts on the NOD-like receptor family, pyrin domain containing 3 (NLRP3) protein that has been shown to be necessary for LZD-mediated bone marrow suppression in mice (16). NLRP3, in conjunction with caspase-1 and ASC, forms an inflammasome complex, which cleaves a number of substrates resulting in cell death and/or the release of active of IL-1β.

While the importance of NLRP3 in bone marrow suppression is clear, the relative roles of inflammasome activation and IL-1 signaling remain uncertain.

Based on these observations, inhibiting the IL-1 pathway by HDT could serve two purposes: first, to alleviate LZD-associated host toxicity, and second, to reduce the pathology associated with the IL-1 pathway during TB disease. Due to the pro-inflammatory nature of the IL-1 pathway, strict regulatory mechanisms exist within the host to quell this pathway. IL-1 receptor antagonist (IL-1Rn) is a protein produced constitutively at low levels that can increase in response to a variety of cytokine signals. IL-1Rn serves as a decoy ligand for the IL-1R1, blocking signal transduction and subduing activation of subsequent pro-inflammatory pathways (17). Anakinra is an FDA-approved recombinant IL-1Rn that is used to treat rheumatoid arthritis. As there are no FDA approved drugs to inhibit inflammasome activation, inhibition of the IL-1 pathway with biologics, such as Anakinra, is the only currently feasible strategy to modulate this pathway (18).

We hypothesized that the combination of Anakinra (herein referred to as IL-1Rn) with LZD for treatment of active TB disease would reduce LZD-associated toxicities and host inflammation resulting in a more efficacious therapy. To test this concept, we employed two established TB animal models to assess differing aspects of host responses to LZD and IL-1Rn. We used multiple strains of mice to model distinct disease states and dissect the relative importance of the inflammasome and IL-1 signaling in HDT efficacy. As a translational model, we used cynomolgus macaques in combination with [^{18}F] FDG PET/CT serial imaging to track TB disease progression, including inflammation, before and during drug regimens (19). Cynomolgus macaques present with a similar spectrum of Mtb infection as humans, with pathology, including granuloma structure and diversity, that recapitulates human TB (20-22). Together, our data further verify LZD as an efficacious antibiotic in both mice and macaques

and indicate that addition of IL-1Rn may accelerate the resolution of inflammation and partially alleviate LZD-mediated BM suppression.

Results

IL-1 receptor blockade reduces inflammation in mouse models of TB disease.

Given the complex role played by IL-1 during TB, we initially sought to determine the effect of inhibiting this cytokine during established TB disease in mice. These studies compared two IL-1 antagonists, a blocking antibody to the murine IL-1 receptor (αIL-1R1) and the human IL-1 receptor antagonist, Anakinra (IL-1Rn), each delivered between days 14 and 28 post infection. Two mouse strains were employed to assess the effects of these treatments in animals with different amounts of IL-1 activity. In relatively resistant C57BL/6 animals, mature IL-1 production is controlled during chronic disease, whereas unregulated IL-1 drives inflammatory disease in Mtb-infected *Nos2*$^{-/-}$ mice (9, 10).

While the human IL-1Rn had little effect in these models, the αIL-1R1 treatment significantly reduced PMN numbers in the lungs of both resistant and susceptible mouse strains, and reversed the weight loss observed in *Nos2*$^{-/-}$ mice (Fig. 1A-B). While neither regimen significantly altered the lung bacterial burden, both IL-1Rn and αIL-1R1 treatment reduced bacterial burden in the spleens of *Nos2*$^{-/-}$ mice (Fig. 1C-D). This generally beneficial effect of αIL-1R1 treatment was consistent with qualitatively improved histopathological disease (Fig. 1E). By no metric did αIL-1R1 treatment exacerbate established disease in either mouse strain.

IL-1 blockade alleviates lung inflammation and hematopoietic suppression during LZD treatment in mice.

The IL-1R1 blocking antibody αIL-1R1 was next tested in combination with LZD to determine whether the efficacy or toxicity of the antibiotic was altered. C3HeB/FeJ mice, which are relatively susceptible to Mtb and develop histopathological lesions that more closely resemble human disease, were used for these studies. Mice with established disease were treated between days 28 and 46 post-infection with vehicle alone, LZD, αIL-1R1 or a combination of the two. As previously reported, LZD was effective in this model, reducing lung neutrophil numbers, bacterial burden and weight loss (Fig. 2 A-D) (23). The addition of αIL-1R1 to this regimen further reduced lung neutrophil numbers, and did not significantly alter the antimicrobial activity of LZD. As IL-1β production in response to both Mtb infection and LZD treatment depends largely on the NLRP3 inflammasome, we also investigated a regimen in which LZD and a small molecule NLRP3 inhibitor (MCC950) was administered between days 56 and 77 post-infection. As observed with αIL-1R1, the addition of MCC950 reduced PMN numbers in the lung, relative to LZD alone, and did not significantly alter the rate of bacterial killing (Fig. 2 E-G). Using a more rapid treatment protocol and C57BL/6 mice with genetic deficiencies in Caspase 1 or NLRP3, we confirmed that the antimicrobial activity of LZD was unaffected by inflammasome activation (Supplementary Fig. 1). Mice were treated between days 14 and 28 post-infection and the effect of LZD on bacterial burden and lung neutrophil number was at least as large in the knockout animals as the wild type controls.

Hematopoietic suppression was assayed in bone marrow and spleens of C3HeB/FeJ mice. Both organs are significant sites for hematopoiesis in small animals, in which the bone marrow has insufficient capacity, particularly when the requirement for blood cells increases. Using flow cytometry, erythroid progenitors can be divided into a progression of precursors; pro-erythrocyte (ProE), EryA, EryB, and EryC (Fig. 3A). These populations were quantified in each tissue of Mtb-infected animals treated with LZD and/or αIL-1R1. In both bone marrow and spleen, LZD

had a profound effect, nearly eliminating early erythroid progenitors of the ProE, EryA and EryB classes (Fig. 3B-E). Simultaneous treatment with αIL-1R1 largely reversed the effect of LZD in the spleen, restoring these immature precursors to approximately half of their untreated levels. While αIL-1R1 also significantly increased the number of erythroid precursors in the BM, the suppression of LZD toxicity was less pronounced at this site.

In sum, studies in the mouse model indicated that the addition of αIL-1R1 to an LZD regimen could reduce the number of lungs PMN and ameliorate hematopoietic toxicity, while not compromising antimicrobial activity. These observations justified further studies in a non-human primate model.

Changes in TB disease in macaques treated with LZD and HDT by PET/CT

Previously we published the efficacy and pharmacokinetics of LZD in cynomolgus macaques treated for 8 weeks with a single daily dose of 30 mg/kg (14). To adhere to FDA guidelines for LZD administration at the time we initiated this study, and reproduce clinical exposure at 600 mg twice daily (b.i.d.), we shortened treatment duration to 4 weeks and increased the dosing frequency to 30 mg/kg b.i.d. Dose finding studies were carried out in uninfected cynomolgus macaques to ensure that adequate drug concentrations similar to those achieved in patients at 600 mg b.i.d. were reached in the blood (Supplementary Fig. 2A).

To assess this HDT/LZD regimen, we infected 10 cynomolgus macaques with Mtb strain Erdman (12 CFU via bronchoscope) and monitored development of active TB disease (~3-5 months) (Supplementary Table 1 and Supplementary Fig. 2B). The macaques were then randomized to a 4-week drug regimen of LZD (n=5) or LZD+IL-1Rn (n=5) (Supplementary Fig. 2B). One advantage of this model is the ability to track disease progression throughout infection

and treatment using serial ^{18}F-FDG PET CT scans (14, 24). Lung inflammation was quantified by total FDG activity in the lungs before and during treatment (Fig. 4A-B and Supplementary Table 1)(19). In LZD treated macaques, there was no significant decrease in total lung FDG activity after 4 weeks (p=0.2876), although there was a trend for an initial reduction in inflammation after 2 weeks of treatment (p=0.0857)(Fig. 4B). In contrast, LZD+IL-1Rn treatment resulted in a significant reduction in total lung FDG activity after 2 and 4 weeks (p=0.0242, p=0.0237 respectively). We assessed changes in granulomas during treatment by measuring physical size (CT) and metabolic activity (measured as the standard uptake value of FDG per granuloma, SUVR) (Fig. 4C-D)(19). During treatment, the majority of granulomas decreased in size with no differences between LZD and LZD+IL1-Rn treated animals. However, granuloma metabolic activity (SUVR) was significantly reduced in LZD+IL-1Rn treated macaques compared to those treated with LZD alone for all granulomas. These data indicate that blocking of IL-1R in combination with LZD reduces inflammation in whole lungs and individual granulomas more effectively than LZD treatment alone.

Supplementary Table 1. List of macaques for study and PET/hot values

Supplemental Table 1 - Macaque Study Data

HDT Study												
NHP	Age (yr)	Gender	Infection Dose	Treatment Group	DPI at Treatment Start	Days of Treatment	DPI at Necropsy	Necropsy Score	Total CFU	PreTx PEThot	2wk PEThot	4wk PEThot
29716	5.9	F	12 CFU	LZD	117	28	145	24	61839	526777.88	58333.57	35664.45
29816	7.1	F	12 CFU	LZD	110	28	138	45	4445	11003.65	1309.29	531.02
30016	7	F	12 CFU	LZD	103	29	132	31	1413	85068.79	123759.67	28665.24
30216	7.1	F	12 CFU	LZD	138	31	169	32	1090	2113.02	401.05	3884.92
30316	7.1	F	12 CFU	LZD	117	30	147	37	8005	1453.44	562.79	1828.43
18816	10.9	M	12 CFU	LZD+IL-1Rn	117	30	147	26	505	3236.21	673.86	1520.78
19116	7.2	M	12 CFU	LZD+IL-1Rn	117	28	145	25	330	3304.52	1469.77	1562.60
19416	9.9	M	12 CFU	LZD+IL-1Rn	138	30	168	10	727	872.50	73.54	73.30
20416	8.2	M	12 CFU	LZD+IL-1Rn	110	31	141	28	1260	26957.57	10456.67	2802.92
30116	6.4	F	12 CFU	LZD+IL-1Rn	103	31	134	67	20905	110837.75	48461.60	7609.82

Historical Controls*						
NHP	Age (yr)	Gender	Infection Dose	DPI at Necropsy	Necropsy Score	Total CFU
18214	8.3	M	39 CFU	84	50	2935647
18314	8.3	M	39 CFU	91	84	1319857
1514	6.2	M	38 CFU	118	56	112433

*PET/CT data previously reported in PMID: 28592427

Provided are details regarding macaques utilized for this study. DPI = days post infection.

Addition of IL-1Rn does not significantly reduce bacterial burden

While IL-1Rn should not have direct bactericidal activity, this agent could still influence the expression of anti-bacterial immunity. This effect could be beneficial if immune responses are enhanced, or detrimental if IL-1 is necessary for host killing of bacteria. Therefore, we performed comprehensive bacterial burden analysis at necropsy, by identifying the majority of granulomas and other TB pathologies on PET CT scans, obtaining each individually at necropsy and culturing all lesions, thoracic lymph nodes, and uninvolved lung tissue separately, as well as extrapulmonary lesions, as previously described (20). Total thoracic CFU (lung + lymph nodes) was not significantly different between LZD and LZD + IL-1Rn macaques ($p = 0.1508$) (Fig. 5A), with similar frequencies of sterilized granulomas (LZD = 68.42%, LZD+IL-1Rn = 72.22%). In the current study, we did not have untreated control macaques, so we provide total thoracic CFU for 3 similarly infected historical controls (untreated) for reference; these data were excluded from statistical analyses. This supports that high dose LZD as a single drug is effective at killing bacteria even in a short (4 week) regimen. Bacterial burden in CFU+ thoracic lymph nodes was similar between the groups though trended towards lower CFU in LZD+IL-1Rn treated macaques ($p=0.0965$) (Fig 5B). We previously reported that a 2-month lower dose regimen of LZD could reduce bacterial burden compared to untreated controls, with ~80% sterilized granulomas (14). Since the bacterial burden in macaques with active TB can vary substantially, we estimated the pre-treatment total thoracic CFU from the total lung FDG by PET CT as previously described (20), and compared the actual bacterial burden post-treatment against the estimated pre-treatment value. All macaques, regardless of treatment group, had lower total thoracic CFU at necropsy compared to the estimated total thoracic CFU prior to treatment initiation (Fig. 5C). Our data indicate that while IL-1Rn did not significantly enhance bacterial killing, it did not impair LZD-mediated bacterial clearance.

Lack of LZD-induced bone marrow suppression in macaques

In humans, LZD is associated with host toxicities during extended treatment periods of > 4 weeks (25). To determine whether bone marrow suppression occurred during the 4-week high dose LZD therapy and whether IL-1Rn could modulate observable host toxicities, we isolated bone marrow at necropsy from the sternum of each macaque and assessed erythropoietic progenitor populations and mitochondrial function by flow cytometry (Fig. 6A). During homeostatic erythropoiesis, a 1:8 ratio is maintained between ProE and EryC populations, which can be used to indicate disruption to erythropoiesis. There was no significant difference in ProE:EryC ratios between the treatment groups or compared to untreated macaques with Mtb infection (Fig. 6B). However, none of the macaque groups had a homeostatic ratio regardless of treatment. These data indicate that Mtb infection or TB disease alone may disrupt bone marrow homeostasis. To determine whether LZD was affecting bone marrow mitochondrial function, we stained cells with MitoTracker™ Red CMXRos that only stains mitochondria with active membrane potential, indicating function of those organelles (Fig. 6B). Regardless of treatment, the MitoTracker MFI remained similar, indicating that mitochondrial function is the same among groups. To confirm our observations, a pathologist evaluated bone marrow tissue sections and found no observable differences between TB only, LZD and LZD+IL-1Rn groups in terms of cellularity (myeloid:erythroid ratios) or abnormalities (Fig. 6C). While we could not consistently identify progenitor populations in blood or spleen, we performed complete blood counts (CBCs) during treatment to identify signs of bone marrow suppression (i.e., anemia, thrombocytopenia). There were no differences between LZD and LZD+IL-1Rn treatments (Supplementary Fig. 3). In conclusion, 4 weeks of LZD was not sufficient to induce observable bone marrow suppression in cynomolgus macaques and blocking of IL-1R did not alter bone marrow status during LZD treatment of TB.

Reduction in inflammatory signatures in the lung after HDT

To determine whether IL-1Rn modulated immune populations in the airway of the lung during treatment, bronchoalveolar lavages (BAL) were acquired prior to the start of treatment and 3 weeks post treatment. Innate and adaptive immune cell populations were identified and frequencies were assessed by flow cytometry (Fig. 7A). Frequencies of CD4 and CD8 T cells (CD3+, CD8+ or CD4+) in BAL remained stable and similar in both groups. Although macrophage (CD11b+CD206+) populations were relatively unchanged, there was a significant reduction in neutrophil (CD11b+, Calprotectin+) frequency in the BAL after 3 weeks of treatment (pooled groups) ($p=0.0098$). This observation was similar to that observed in mice (Fig 2A). To determine whether the cytokine milieu in the airways changed during treatment, a subset of 3 animals per group were chosen at random for analysis by multi-plex using 10X concentrated BAL fluid (Fig. 7B). Given the small subset, statistical analysis was performed on combined treatment groups to only compare pre and post treatment changes. We assessed IL-1β and IL-1RA as IL-1Rn may modulate this pathway and saw no significant changes after treatment (IL-1β $p=0.1562$, IL-1RA $p=0.1250$). Interferon-inducible T cell alpha chemoattractant (I-TAC) is upregulated in response in interferons and IL-1 and is generally an indicator of inflammation, which also trended towards reduced levels post treatment, however was not statistically significant ($p=0.0625$). IL-8, a neutrophil chemoattractant, was significantly reduced after treatment, mirroring the reduction in neutrophil frequency observed by flow cytometry and mouse data. These data suggest that treatment with either LZD or LZD+IL-1Rn rapidly reduces inflammatory signatures associated with TB disease in the airways.

IL-1 blockade modulates granuloma specific responses and healing dynamics

To determine whether IL-1Rn modulated immune responses at the site of infection, we chose at random 5 granulomas per animal (25 per treatment group) and performed a multi-plex analysis of granuloma supernatants (Fig. 8A). There were no significant differences in IL-1β, IL-1RA, or

IL-18 levels, which are associated with the IL-1 pathway. IL-2 and IL-17 are correlated with protective immune responses during TB (26); there was a trend for higher IL-2 levels in LZD+IL-1Rn treatment and a statistically significant increase in IL-17a in LZD+IL-1Rn treated animals. G-CSF/CSF-3 levels were significantly higher in LZD+IL-1Rn treated granulomas, providing further evidence of IL-1Rn immune modulation. The IL-1 pathway is associated with fibrosis, which increases in granulomas during drug treatment. IL-17 and G-CSF are also associated with fibrosis (27). Granulomas suitable for histological analysis were evaluated by a blinded pathologist and lesions were categorized based on treatment groups and descriptive qualities (Fig. 8B). Of lesions acquired from LZD only animals, 71.43% were deemed fibrotic (n= 40/56), while those with the addition of IL-1Rn had 84.78% fibrotic lesions (n=39/46) with no significant difference in frequency of fibrotic lesions between treatment groups. We also compared the number and frequency of granulomas that were deemed necrotizing or non-necrotizing ("other" indicates neither categorization). Granulomas from LZD+IL-1Rn treated animals had significantly more non-necrotizing granulomas (73.91%, n=34/46), compared to those from LZD alone treated macaques (46.43%, n=26/56). The proportion of necrotizing granulomas was significantly lower in the LZD+IL-1Rn treatment group (13.04%, n=6/56) compared to LZD alone (30.36%, n=17/56) (p=0.0151). These data suggest that addition of IL-1Rn may influence antibiotic-associated healing dynamics of granulomas.

Discussion

HDTs are a tantalizing solution in combating drug-resistant pathogens, however the complexities of host-pathogen interactions and host variability call for rigorous pre-clinical testing before implementation in humans. Here, we sought to determine the efficacy and safety of an HDT for TB comprised of LZD and IL-1Rn. IL-1 has a complex role during TB, as IL-1 is important for early control of infection, yet damaging in later

331 stages of disease. To validate the safety of IL-1Rn in this context, we first assessed the
332 effects of IL-1Rn on TB disease progression in mice. Using αIL-1R1 blockade,
333 antagonism of IL-1R1 did not exacerbate disease and reduced PMN infiltrates which are
334 associated with pathological inflammation. While inhibition of IL-1 signaling during the
335 early stages of infection has been shown to potentiate disease, the beneficial effect of
336 IL-1 inhibition that we observed in multiple mouse models of TB highlights the generally
337 pathological role for this cytokine during established infections (7, 8).
338 When co-administered with LZD, blockade of IL-1R1 reduced PMN infiltrates in the
339 mouse models, compared to the antibiotic alone. Similarly, IL-1Rn reduced
340 inflammation in the granulomas of macaques, as well as overall lung inflammation as
341 assessed by PET CT, but did not significantly enhance bacterial clearance. A trend of
342 lower CFU in CFU+ lymph nodes ($p=0.0965$) was observed from macaques treated with
343 LZD+IL-1Rn compared to LZD alone. We hypothesize that IL-1Rn may reduce
344 inflammation in tissues to allow for enhanced penetration of LZD to reduce bacterial
345 burden in tissues. Given that lymph nodes are a site of Mtb persistence, this finding is
346 worth further exploration as a means of potentially enhancing drug penetration in
347 tissues (28).
348
349 In the BAL, we observed a decrease in neutrophils (PMNs) during HDT and a
350 corresponding decrease in IL-8 in both treatment group (LZD or LZD+IL-1Rn), indicating
351 LZD alone was efficacious in reducing PMN inflammatory signatures, likely due to the
352 reduction in bacterial burden. In granulomas, levels of IL-1β, IL-1RA and IL-18 were not
353 affected by IL-1Rn treatment in the subset examined. As IL-1Rn does not affect

354 inflammasome formation and function, only IL-1R1 signal transduction, it is not
355 surprising that IL-1β and IL-18 production were not affected by IL-1Rn. Of the 30
356 cytokines and chemokines assessed, IL-2, IL-17A and G-CSF were the most modulated
357 after IL-1Rn treatment. IL-2 and IL-17A have protective functions during TB and are
358 primarily expressed by T cells (26). While IL-1β has been reported to enhance IL-17A
359 production by T cells in mice, these studies primarily have utilized model-antigen
360 systems while our study reflects a chronic infection model (29). IL-1 is known to be
361 protective early during Mtb infection while exacerbating pathology during later infection,
362 highlighting that the effects of IL-1 on adaptive immunity are complex and likely
363 dependent on the host and infection model. G-CSF was increased in granulomas from
364 LZD+IL-1Rn treated macaques which, combined with our observations of reduced PMN
365 infiltrates in mouse lungs and macaque airways, indicated a paradoxical role of G-CSF
366 as a neutrophil production and differentiation factor (30). However, in a model of LPS-
367 induced lung injury it was shown that G-CSF blockade induced accumulation of PMNs
368 and increased inflammation in the lungs, indicating pulmonary inflammation may not
369 follow dogmatic rules of canonical inflammatory pathways (30).
370
371 Fibrosis is modulated by the IL-1 pathway, however while fibrosis is associated with
372 granuloma healing, lung fibrosis can cause secondary complications after TB disease
373 resolution (2) . We have shown in previous studies that drug therapy for TB induces
374 fibrotic healing in granulomas (31, 32). Therefore, we assessed whether IL-1Rn was
375 associated with changes in granuloma pathology. While we did not observe a
376 significant difference in the frequency of fibrotic versus non-fibrotic granulomas

(p=0.1531), there was a significant decrease in necrotizing granulomas when IL-1Rn was added to LZD therapy. Thus, although there is no synergistic effect between IL-1Rn and LZD in promoting fibrosis associated with drug clearance, the reduction in neutrophils could skew granuloma resolution towards a non-necrotizing, fibrotic lesion.

We also assessed LZD-associated bone marrow suppression and reversal with IL-1Rn therapy. We designed our HDT to match the current FDA guidelines for LZD and IL-1Rn schedules, which resulted in a lack of observable bone marrow suppression in macaques. In mice however, LZD-induced bone marrow suppression was reduced with the addition of IL-1R1 antagonists, supporting our initial hypothesis. The role of IL-1 signaling is consistent with the ability of IL-1 to suppress erythropoiesis in mice by reducing the number of progenitors (33). The remaining deficit in erythropoiesis during IL-1 blockade could reflect either incomplete inhibition by IL-1Rn or an independent role of inflammasome activation. Optimizing this effect will require further work to understand the relative roles of IL-1 signaling and inflammasome activation.

Our data support and extend our previous data in macaques that LZD has excellent efficacy against TB, even as a single-drug given for only 4-weeks, providing additional support for LZD as an antimicrobial for MDR/XDR-TB cases (12). IL-1Rn therapy in conjunction with LZD was successful in reducing TB-associated inflammation with no negative effects on Mtb clearance, however additional studies addressing long-term effects on immune responses and TB disease resolution are needed. Anakinra (IL-1Rn) is already FDA-approved for adult and pediatric use in other inflammatory disorders; our

data provide pre-clinical evidence that IL-1Rn could be a potential therapy for cases of severe TB to quell excessive inflammation and improve standard therapies. Our study highlights the potential of HDTs for TB but also the necessity of assessment in translational models prior to implementation in human trials.

Methods

Ethics Statement

All experimental manipulations, protocols, and care of the animals were approved by the University of Pittsburgh School of Medicine Institutional Animal Care and Use Committee (IACUC). The protocol assurance number for our IACUC is A3187-01. Our specific protocol approval numbers for this project are 15117082, 16017370, 18124275, 13011368 and 16027525. The IACUC adheres to national guidelines established in the Animal Welfare Act (7 U.S.C. Sections 2131 - 2159) and the Guide for the Care and Use of Laboratory Animals (8th Edition) as mandated by the U.S. Public Health Service Policy.

All macaques used in this study were housed at the University of Pittsburgh in rooms with autonomously controlled temperature, humidity, and lighting. Animals were singly housed in caging at least 2 square meters that allowed visual and tactile contact with neighboring conspecifics. The macaques were fed twice daily with biscuits formulated for nonhuman primates, supplemented at least 4 days/week with large pieces of fresh fruits or vegetables. Animals had access to water *ad libitem*. Because our macaques were singly housed due to the infectious nature of these studies, an enhanced enrichment plan was designed and overseen by our nonhuman primate enrichment

423 specialist. This plan has three components. First, species-specific behaviors are
424 encouraged. All animals have access to toys and other manipulata, some of which will
425 be filled with food treats (e.g. frozen fruit, peanut butter, etc.). These are rotated on a
426 regular basis. Puzzle feeders foraging boards, and cardboard tubes containing small
427 food items also are placed in the cage to stimulate foraging behaviors. Adjustable
428 mirrors accessible to the animals stimulate interaction between animals. Second,
429 routine interaction between humans and macaques are encouraged. These interactions
430 occur daily and consist mainly of small food objects offered as enrichment and adhere
431 to established safety protocols. Animal caretakers are encouraged to interact with the
432 animals (by talking or with facial expressions) while performing tasks in the housing
433 area. Routine procedures (e.g. feeding, cage cleaning, etc) are done on a strict
434 schedule to allow the animals to acclimate to a routine daily schedule. Third, all
435 macaques are provided with a variety of visual and auditory stimulation. Housing areas
436 contain either radios or TV/video equipment that play cartoons or other formats
437 designed for children for at least 3 hours each day. The videos and radios are rotated
438 between animal rooms so that the same enrichment is not played repetitively for the
439 same group of animals.

440 All animals are checked at least twice daily to assess appetite, attitude, activity
441 level, hydration status, etc. Following *M. tuberculosis* infection, the animals are
442 monitored closely for evidence of disease (e.g., anorexia, weight loss, tachypnea,
443 dyspnea, coughing). Physical exams, including weights, are performed on a regular
444 basis. Animals are sedated prior to all veterinary procedures (e.g. blood draws, etc.)
445 using ketamine or other approved drugs. Regular PET/CT imaging is conducted on

most of our macaques following infection and has proved very useful for monitoring disease progression. Our veterinary technicians monitor animals especially closely for any signs of pain or distress. If any are noted, appropriate supportive care (e.g. dietary supplementation, rehydration) and clinical treatments (analgesics) are given. Any animal considered to have advanced disease or intractable pain or distress from any cause is sedated with ketamine and then humanely euthanatized using sodium pentobarbital.

Mice, infection and treatment

C57BL/6 (stock no. 000664), *Nos2*$^{-/-}$ (B6.129P2-Nos2^{tm1Lau}/J, stock no. 002609), C3HeB/FeJ (stock no. 00658), and *Nlrp3*$^{-/-}$ (B6.129S6-*Nlrp3*^{tm1Bhk}/J, stock no. 021302) were purchased from the Jackson Laboratory. Breeding pairs of Caspase-1/11 double knock out mice were kindly provided by Prof. Katherine Fitzgerald of the Department of Infectious Diseases at University of Massachusetts (UMASS) Medical School and bred in house. Mice were housed under specific pathogen-free conditions, and in accordance with the UMASS Medical School, IACUC guidelines. All mouse strains used in this study were of C57BL/6 background unless otherwise indicated.

The wild type strain of *M. tuberculosis* (Mtb) Erdman was used in these studies. Bacteria were cultured in 7H9 medium containing 0.05% Tween 80 and OADC enrichment (Becton Dickinson). For infections, mycobacteria were suspended in phosphate-buffered saline (PBS)-Tween 80 (0.05%); clumps were dissociated by sonication, and ~100 CFU were delivered via the respiratory route using an aerosol generation device (Glas-Col, Terre Haute, IN). At indicated time points mice were treated with 200mg/kg of Linezolid (LZD). These drugs were prepared in 0.5% carboxymethyl cellulose (CMC) and Polyethylene glycol 300 solution as the vehicle. Cohorts of

mice were treated with anti-IL-1R1 antibody (InVivoMab, anti-mouse IL-1R, Clone JAMA147, BioXcell), or human recombinant IL-1 receptor antagonist (IL-1Rn, Kineret™) either alone or in combination with LZD. 0.5% CMC and Polyethylene glycol was used as vehicle control. All antibiotic treatment was done by daily oral gavage. Anti-IL-1R1 (100ug/mouse/0.2mL) was administered every alternate day by subcutaneous and intraperitoneal route. IL-1Rn (Kineret) was administered (25mg/kg/mouse) everyday by subcutaneous route.

Macaque pharmacokinetic study and analytical method.

Uninfected macaques designated for other studies (n=3) were given 20mg/kg or 40mg/kg by oral gavage and plasma acquired at 0, 5, 19, 15, 20, 25 and 30 hours post LZD administration. High pressure liquid chromatography coupled to tandem mass spectrometry (LC/MS-MS) analysis was performed on a Sciex Applied Biosystems Qtrap 4000 triple-quadrupole mass spectrometer coupled to an Agilent 1260 HPLC system to quantify LZD in macaque plasma. LZD chromatography was performed on an Agilent Zorbax SB-C8 column (2.1x30 mm; particle size, 3.5 µm) using a reverse phase gradient elution. Milli-Q deionized water with 0.1% formic acid was used for the aqueous mobile phase and 0.1% formic acid in acetonitrile for the organic mobile phase. Multiple-reaction monitoring (MRM) of parent/daughter transitions in electrospray positive-ionization mode was used to quantify the analytes. Sample analysis was accepted if the concentrations of the quality control samples were within 20% of the nominal concentration. Data processing was performed using Analyst software (version 1.6.2; Applied Biosystems Sciex).

Neat 1 mg/mL DMSO stocks for all compounds were serial diluted in 50/50 Acetonitrile water to create standard curves and quality control spiking solutions. 20 µL of neat spiking solutions were added to 20 µL of drug free plasma or control tissue homogenate, and extraction was performed by adding 180 µL of Acetonitrile/Methanol 50/50 protein precipitation solvent containing the internal standard (10 ng/mL verapamil & deuterated LZD-d3). Extracts were vortexed for 5

minutes and centrifuged at 4000 RPM for 5 minutes. 100 µL or supernatant was transferred for LC-MS/MS analysis and diluted with 100 µL of Milli-Q deionized water.

Rhesus macaque plasma (Lithium Heparin, Bioreclamation IVT, NY) was used as a surrogate to cynomolgus macaque plasma to build standard curves. LZD-d3 internal standard and verapamil were purchased from Toronto Research Chemical. The lower and upper limits of quantitation (LLOQ and ULOQ) were 1 ng/mL and 50,000 ng/mL respectively. The following MRM transitions were used for LZD (338.00/235.00), LZD-d3(341.20/297.20), and verapamil (455.40/165.20).

Macaques, infection and treatment

All housing, care, and experimental procedures were approved by the University of Pittsburgh School of Medicine Institutional Animal Care and Use Committee (IACUC). Examination of animals was performed in quarantine to assess physical health and confirmation of no previous *M. tuberculosis* infections as previously described (34). Cynomolgus macaques (*Macaca fascicularis*) (N=10) were purchased for this study from (Valley Biosystems). Bone marrow control (non-drug treated) samples were taken from Mtb-infected cynomolgus macaques in unrelated ongoing studies (N=5). For the current study, all 10 animals were infected bronchoscopically with 12 CFU of Mtb strain Erdman. After active disease developed (3-5 months), NHPs were randomized to LZD only (N=5) or LZD+IL-1Rn (N=5) treatment groups. For randomization, macaques were paired based on total FDG activity in lungs (a surrogate for total thoracic CFU), and then assigned to treatment by coin flip (20). LZD was administered twice a day orally with food (30mg/kg), while IL1-Rn was given at 2mg/kg once each day by subcutaneous injection. All animal data are provided in Supplementary Table 1. Medication compliancy was monitored at every administration and pharmacokinetic analysis performed at select times. Drug treatments were administered for 4 weeks prior to necropsy. Bronchoalveolar lavages (BAL) were performed prior to drug-treatment and 3 weeks-post start of treatment for CFU, flow cytometry and multiplex assays.

522

523 **Macaque PET/CT Imaging**

524 Positron emission tomography (PET) with computed tomography (CT) imaging was performed
525 with 2-deoxy-2-[^{18}F]-D-deoxyglucose (FDG) throughout the study as previously described (19).
526 Serial scans were performed throughout the study to track disease progression and changes
527 during drug treatment. Total FDG activity of the lungs was measured over the course of
528 infection and drug treatment as previously described (19). Granulomas identified on scans were
529 denoted, measured (mm) and standard uptake values (SUVR) were determined to assess
530 metabolic activity, a readout for inflammation. SUVR values were normalized to muscle and
531 SUVR and size measurements were determined at each scan over time to compare pre-and
532 post-drug treatment. Each animal was scanned prior to necropsy to identify granulomas for
533 matching at necropsy; granulomas $\geq$ 1mm are distinguishable by PET/CT.

534

535 **Macaque Necropsy**

536 Necropsies were performed as previously described. In short, multiple tissues (granulomas, lung
537 lobes, thoracic lymph nodes, peripheral lymph nodes, liver, spleen, bone marrow) were excised
538 and homogenized into single-cell suspensions for assessment of bacterial burden and
539 immunological assays. Granulomas were individually excised (PET/CT identified and others not
540 identified on scans) and split (size permitting) with one-half for homogenization and single cell
541 suspension and the other half processed for histological analysis. Bone marrow samples were
542 obtained from the sternum, with a portion sent for histological analysis while single cell
543 suspensions were acquired as previously described (35). Bacterial burden was assessed from
544 each tissue by plating serial dilutions on 7H11 agar plates and incubated at 37°C in 5% CO_2 for
545 21 days before enumeration of Mtb CFU.

546

547 **Flow cytometry and Immunoassays**

548 **Mice**. Single cell suspensions were prepared from the infected mouse organs. Briefly, lung tissue
549 was digested with Collagenase type IV/DNaseI and passed through 40 μm cell strainers to obtain
550 single cell suspension. Red blood cells were lysed using Tris-buffered Ammonium Chloride (ACT)
551 Non-specific antibody binding sites were blocked by Fc-Block CD16/32 (Clone 93, cat. no.
552 101319) and the cells were stained with anti-CD3-PE (Clone 17A2, cat. no. 100205), anti-CD11b-
553 PerCP Cy5.5 (Clone M1/70, cat. no.101227), anti-Ly-6G-FITC (Clone 1A8, cat. no.127605), anti-
554 Ly-6C-PE (Clone HK1.4, cat. no.128007), anti-Gr1-APC (Clone RB6-8C5, cat. no.108411), anti-
555 Ter119-PE (Clone TER119, cat. no.116208), anti-CD71-FITC (clone RI7217, cat. no. 113806).
556 Antibodies were purchased from BioLegend. All analyses were performed on live cells only after
557 staining them with fixable live dead stain conjugated with eFlour780, purchased from
558 eBiosciences. All the staining was done according to the manufacturer's instructions. Lung,
559 spleen and bone marrow cells were surface stained for 30 minutes at room temperature, fixed for
560 20 minutes at 4^0C using the Cytofix buffer (BD-Biosciences, cat. no. 554655). Data were acquired
561 in a BD LSRII flow cytometer in the flow cytometry core facility at UMASS medical school and
562 analyzed with FlowJo Software (Treestar, Inc.). Gating strategies are provided in applicable
563 figures.
564 **Macaques.** Single cell suspensions acquired from homogenization of granulomas, lung lobes
565 and lymph nodes were subjected to intracellular cytokine staining (ICS). Prior to staining, cells
566 were incubated in RPMI 1640 containing 1% HEPES, 1% L-glutamine, 10% human AB serum,
567 and 0.1% brefeldin A (Golgiplug; BD Biosciences) for 3 h at 37°C in 5% CO_2. After viability
568 staining (Invitrogen), surface antigens and intracellular cytokines were assessed using standard
569 protocols. Surface markers include CD3 (SP34-2; BD Pharmingen), CD4 (L200; BD Horizon),
570 CD8 (RPA-T8; BD Horizon) for T cells and CD11b (ICRF44; BD Pharmingen), CD206 (19.2; BE
571 Pharmingen) for macrophages/neutrophils. Calprotectin (27E10; ThermoFisher) was stained
572 intracellularly to identify neutrophils. For bone marrow, single cell suspensions underwent red
573 blood cell lysis (BD Pharm Lyse) before incubation in alpha-MEM + 10% Stasis™ FBS (Gemini

Bio-Products) + MitoTracker™ Red CMXRos (Invitrogen) for 30 minutes to stain for membrane potential of mitochondria. Cells were then stained for viability (Invitrogen) and surface stained to distinguish erythroid progenitor populations by CD34 (581; Biolegend), CD235a (HIR2; BD Pharmingen), CD71 (L01.1; BD Pharmingen) and CD45 (D058-1283; BD Pharmingen). All samples were acquired on an LSR II (BD) and analyzed with FlowJo Software (Treestar, Inc.). Gating strategies are provided in applicable figures.

For the multiplex assays, all samples and supernatants were stored at -80°C from time of necropsy until time of assay. Five representative granuloma supernatants were randomly selected from each animal using JMP Pro v12 (SAS Institute Inc.). Supernatants were thawed and filtered with a 0.22uM syringe filter to remove infectious bacteria and debris, then kept on ice throughout the assay. For BAL samples, supernatants were concentrated using regenerated cellulose centrifugal filter tubes (3,000 NMWL, Millipore Sigma) to a final 10X concentration (5mL to 0.5mL). Both granuloma and BAL supernatants were evaluated with a ProcartaPlex multiplex immunoassay (Invitrogen) that assesses thirty cytokines and chemokines specific for NHPs. We followed the manufacturer's protocol with one modification in which we diluted the standard out an extra dilution to increase the range of detection. Results were analyzed by a BioPlex reader (BioRad).

Histopathology and immunofluorescence

Mice. Lung tissues were fixed in 10% buffered formalin and embedded in paraffin. Five micrometer-thick sections were stained with hematoxylin and eosin (H&E). Tissue staining was done by the Diabetes and Endocrinology Research Center histopathology core facility at the University of Massachusetts Medical School or immunology core facility of Albany medical college, NY. Brightfield images were acquired in Abaxis VETSCAN HD microscope.

Paraffin embedded lung tissue sections were cut at 5 µm thickness, mounted on ultraclean glass slides covered in silane, deparaffinized, then dehydrated and rehydrated using the following

steps: Ethanol solutions (30, 50, 70, 90, 95 and 100 % for 3 min each), xylenes (2 different solutions for 10 min each) and ethanol solutions (100, 95, 90, 70, 50 and 30 for 3 min each). The slides were washed once in Tris buffer saline (TBS) for 5 min. Slices were subjected to antigen retrieval by boiling in sodium citrate buffer at pH=6.0 for 20 min and incubated in 0.1% Triton-X 100 for 5 min. Slices were removed and allowed to equilibrate to room temperature for at least 20 min, and rinsed with distilled water. Tissue sections were blocked (blocking solution; 0.5 M EDTA, 1% BSA, in PBS) and incubated overnight in primary antibodies against the proteins related to our studies. Sections were stained for nuclei (DAPI, blue staining), anti-mouse CD3e (cat.no. ab16669, green staining), anti-mouse Ly-6G (clone 1A8, cat. no. 127602) to identify neutrophil granulocytes (Cy3, red staining). As controls, pre-immune serum and isotype matched controls were used. After incubation, the tissues were washed several times with sterile TBS at room temperature and incubated in the respective secondary antibodies (anti-rabbit conjugated to Alexa-488, anti-rat conjugated to Cy3) for at least 2h at room temperature. Tissue sections were mounted using Prolong Gold Antifade reagent (Invitrogen, grand Island, NY) with DAPI, and the tissue sections were examined in ECHO Revolve 4 microscope. Isotype matched control antibodies were used for checking antibody specificity.

Macaques. As previously described, samples acquired at necropsy were formalin fixed, paraffin embedded, cut into ~5μm serial sections and stained with H&E (34). A study-blinded veterinary pathologist assessed and characterized each granuloma, indicating size, type, distribution and cellular composition. Sterna for bone marrow analysis were excised and formalin fixed then transected longitudinally into 1 to 2 sternebral unites and placed in Cal-Ex Hydrochloric acid decalcification solution for 2-4 hours. Upon removal, specimens were washed and trimmed to test for adequate mineral removal, then submitted for routine tissue processing with other tissue specimens as described above.

Statistical Analysis

Mouse studies: Equal variance between samples was assessed by Brown-Forsythe test. Experiments in which variances were equivalent were analyzed by one-way ANOVA with Sidak's multiple comparisons test. Those with unequal variances were analyzed by Welch ANOVA and Dunnett's multiple comparisons test. P values < 0.05 was considered significant. **Macaque studies:** Nonparametric U tests (Mann-Whitney) were performed for two-group comparisons and Kruskal-Wallis tests were performed for three-group comparisons as indicated on data sets with non-normal distributions. Wilcoxon signed rank tests were performed for matched pairs. Fisher's exact test was run on any categorical data. P values < 0.05 were considered significant. Total lung FDG activity was $\log_{10}$-transformed. A two-way ANOVA was utilized to test whether treatment or time (or an interaction between these factors) had an effect on total lung inflammation. Dunnett's multiple comparison tests were then used to compare each time point to pre-drug treatment within each treatment group. Statistical analyses were performed in GraphPad Prism 8 (GraphPad Software, San Diego, CA). A regression equation created from control animals from previous studies was used to create a 95% prediction interval for total thoracic bacterial burden using total lung FDG activity on the scan just before drug treatment (20). The lower and upper bounds and the mean of this prediction interval were subtracted from each animal's total CFU to estimate change in CFU over the course drug treatment. All statistical analyses are referenced in the corresponding figure legends.

Acknowledgements

These studies were funded by NIH UH2AI122295 (JLF and CMS). CGW was supported by NIH T32AI049820. We thank all members of the Flynn, Sassetti, Mattila, and Lin laboratories for their collaborative efforts during this study. We are grateful for intellectual contributions from Dr. Clifton Barry III and Dr. Robert Wilkinson. Special thanks to all the veterinary and research staff for their efforts, expertise and dedication to these studies.

651

652 ## References

653 1. WHO. Global Tuberculosis Report 2018. 2018.

654 2. Pasipanodya JG, Miller TL, Vecino M, Munguia G, Garmon R, Bae S, et al. Pulmonary

655 impairment after tuberculosis. Chest. 2007;131(6):1817-24.

656 3. Tobin DM. Host-Directed Therapies for Tuberculosis. Cold Spring Harb Perspect Med.

657 2015;5(10).

658 4. Baindara P. Host-directed therapies to combat tuberculosis and associated non-

659 communicable diseases. Microb Pathog. 2019;130:156-68.

660 5. Fremond CM, Togbe D, Doz E, Rose S, Vasseur V, Maillet I, et al. IL-1 Receptor-

661 Mediated Signal Is an Essential Component of MyD88-Dependent Innate Response to

662 Mycobacterium tuberculosis Infection. The Journal of Immunology. 2007;179(2):1178-89.

663 6. Di Paolo NC, Shafiani S, Day T, Papayannopoulou T, Russell DW, Iwakura Y, et al.

664 Interdependence between Interleukin-1 and Tumor Necrosis Factor Regulates TNF-Dependent

665 Control of Mycobacterium tuberculosis Infection. Immunity. 2015;43(6):1125-36.

666 7. Juffermans NP, Florquin S, Camoglio L, Verbon A, Kolk AH, Speelman P, et al.

667 Interleukin-1 signaling is essential for host defense during murine pulmonary tuberculosis. J

668 Infect Dis. 2000;182(3):902-8.

669 8. Mayer-Barber KD, Andrade BB, Barber DL, Hieny S, Feng CG, Caspar P, et al. Innate

670 and adaptive interferons suppress IL-1alpha and IL-1beta production by distinct pulmonary

671 myeloid subsets during Mycobacterium tuberculosis infection. Immunity. 2011;35(6):1023-34.

672 9. Mishra BB, Lovewell RR, Olive AJ, Zhang G, Wang W, Eugenin E, et al. Nitric oxide

673 prevents a pathogen-permissive granulocytic inflammation during tuberculosis. Nat Microbiol.

674 2017;2:17072.

675 10. Mishra BB, Rathinam VA, Martens GW, Martinot AJ, Kornfeld H, Fitzgerald KA, et al.
676 Nitric oxide controls the immunopathology of tuberculosis by inhibiting NLRP3 inflammasome-
677 dependent processing of IL-1beta. Nat Immunol. 2013;14(1):52-60.
678 11. Zhang G, Zhou B, Li S, Yue J, Yang H, Wen Y, et al. Allele-specific induction of IL-1beta
679 expression by C/EBPbeta and PU.1 contributes to increased tuberculosis susceptibility. PLoS
680 Pathog. 2014;10(10):e1004426.
681 12. Maxmen A. Treatment for extreme drug-resistant tuberculosis wins US government
682 approval. Nature 2019.
683 13. Tan TQ, Yogev R. Clinical pharmacology of linezolid: an oxazolidinone antimicrobial
684 agent. Expert Rev Clin Pharmacol. 2008;1(4):479-89.
685 14. Coleman MT, Chen RY, Lee M, Lin PL, Dodd LE, Maiello P, et al. PET/CT imaging
686 reveals a therapeutic response to oxazolidinones in macaques and humans with tuberculosis.
687 Sci Transl Med. 2014;6(265):265ra167.
688 15. Lee M, Lee J, Carroll MW, Choi H, Min S, Song T, et al. Linezolid for treatment of
689 chronic extensively drug-resistant tuberculosis. N Engl J Med. 2012;367(16):1508-18.
690 16. Iyer SS, He Q, Janczy JR, Elliott EI, Zhong Z, Olivier AK, et al. Mitochondrial cardiolipin
691 is required for Nlrp3 inflammasome activation. Immunity. 2013;39(2):311-23.
692 17. Weber A, Wasiliew P, Kracht M. Interleukin-1 (IL-1) pathway. Sci Signal.
693 2010;3(105):cm1.
694 18. Furst DE. Anakinra: review of recombinant human interleukin-I receptor antagonist in the
695 treatment of rheumatoid arthritis. Clin Ther. 2004;26(12):1960-75.
696 19. White AG, Maiello P, Coleman MT, Tomko JA, Frye LJ, Scanga CA, et al. Analysis of
697 18FDG PET/CT Imaging as a Tool for Studying Mycobacterium tuberculosis Infection and
698 Treatment in Non-human Primates. J Vis Exp. 2017(127).

699 20. Maiello P, DiFazio RM, Cadena AM, Rodgers MA, Lin PL, Scanga CA, et al. Rhesus
700 Macaques Are More Susceptible to Progressive Tuberculosis than Cynomolgus Macaques: a
701 Quantitative Comparison. Infect Immun. 2018;86(2).
702 21. Lin PL, Maiello P, Gideon HP, Coleman MT, Cadena AM, Rodgers MA, et al. PET CT
703 Identifies Reactivation Risk in Cynomolgus Macaques with Latent M. tuberculosis. PLoS
704 Pathog. 2016;12(7):e1005739.
705 22. Cadena AM, Fortune SM, Flynn JL. Heterogeneity in tuberculosis. Nat Rev Immunol.
706 2017;17(11):691-702.
707 23. Driver ER, Ryan GJ, Hoff DR, Irwin SM, Basaraba RJ, Kramnik I, et al. Evaluation of a
708 mouse model of necrotic granuloma formation using C3HeB/FeJ mice for testing of drugs
709 against Mycobacterium tuberculosis. Antimicrob Agents Chemother. 2012;56(6):3181-95.
710 24. Lin PL, Coleman T, Carney JP, Lopresti BJ, Tomko J, Fillmore D, et al. Radiologic
711 Responses in Cynomolgus Macaques for Assessing Tuberculosis Chemotherapy Regimens.
712 Antimicrob Agents Chemother. 2013;57(9):4237-44.
713 25. Fung HB, Kirschenbaum HL, Ojofeitimi BO. Linezolid: an oxazolidinone antimicrobial
714 agent. Clin Ther. 2001;23(3):356-91.
715 26. Gideon HP, Phuah J, Myers AJ, Bryson BD, Rodgers MA, Coleman MT, et al. Variability
716 in tuberculosis granuloma T cell responses exists, but a balance of pro- and anti-inflammatory
717 cytokines is associated with sterilization. PLoS Pathog. 2015;11(1):e1004603.
718 27. Borthwick LA. The IL-1 cytokine family and its role in inflammation and fibrosis in the
719 lung. Semin Immunopathol. 2016;38(4):517-34.
720 28. Ganchua SKC, Cadena AM, Maiello P, Gideon HP, Myers AJ, Junecko BF, et al. Lymph
721 nodes are sites of prolonged bacterial persistence during Mycobacterium tuberculosis infection
722 in macaques. PLoS Pathog. 2018;14(11):e1007337.

723 29. Ben-Sasson SZ, Hu-Li J, Quiel J, Cauchetaux S, Ratner M, Shapira I, et al. IL-1 acts
724 directly on CD4 T cells to enhance their antigen-driven expansion and differentiation. Proc Natl
725 Acad Sci U S A. 2009;106(17):7119-24.
726 30. Bajrami B, Zhu H, Kwak HJ, Mondal S, Hou Q, Geng G, et al. G-CSF maintains
727 controlled neutrophil mobilization during acute inflammation by negatively regulating CXCR2
728 signaling. J Exp Med. 2016;213(10):1999-2018.
729 31. DiFazio RM, Mattila JT, Klein EC, Cirrincione LR, Howard M, Wong EA, et al. Active
730 transforming growth factor-beta is associated with phenotypic changes in granulomas after drug
731 treatment in pulmonary tuberculosis. Fibrogenesis Tissue Repair. 2016;9:6.
732 32. Warsinske HC, DiFazio RM, Linderman JJ, Flynn JL, Kirschner DE. Identifying
733 mechanisms driving formation of granuloma-associated fibrosis during Mycobacterium
734 tuberculosis infection. J Theor Biol. 2017;429:1-17.
735 33. Johnson CS, Pourbohloul SC, Furmanski P. Negative regulators of in vivo
736 erythropoiesis: interaction of IL-1 alpha and TNF-alpha and the lack of a strict requirement for T
737 or NK cells for their activity. Exp Hematol. 1991;19(2):101-5.
738 34. Lin PL, Pawar S, Myers A, Pegu A, Fuhrman C, Reinhart TA, et al. Early events in
739 Mycobacterium tuberculosis infection in cynomolgus macaques. Infect Immun. 2006;74(7):3790-
740 803.
741 35. Phuah JY, Mattila JT, Lin PL, Flynn JL. Activated B cells in the granulomas of nonhuman
742 primates infected with Mycobacterium tuberculosis. Am J Pathol. 2012;181(2):508-14.

743

744 ## Figures and Figure Legends

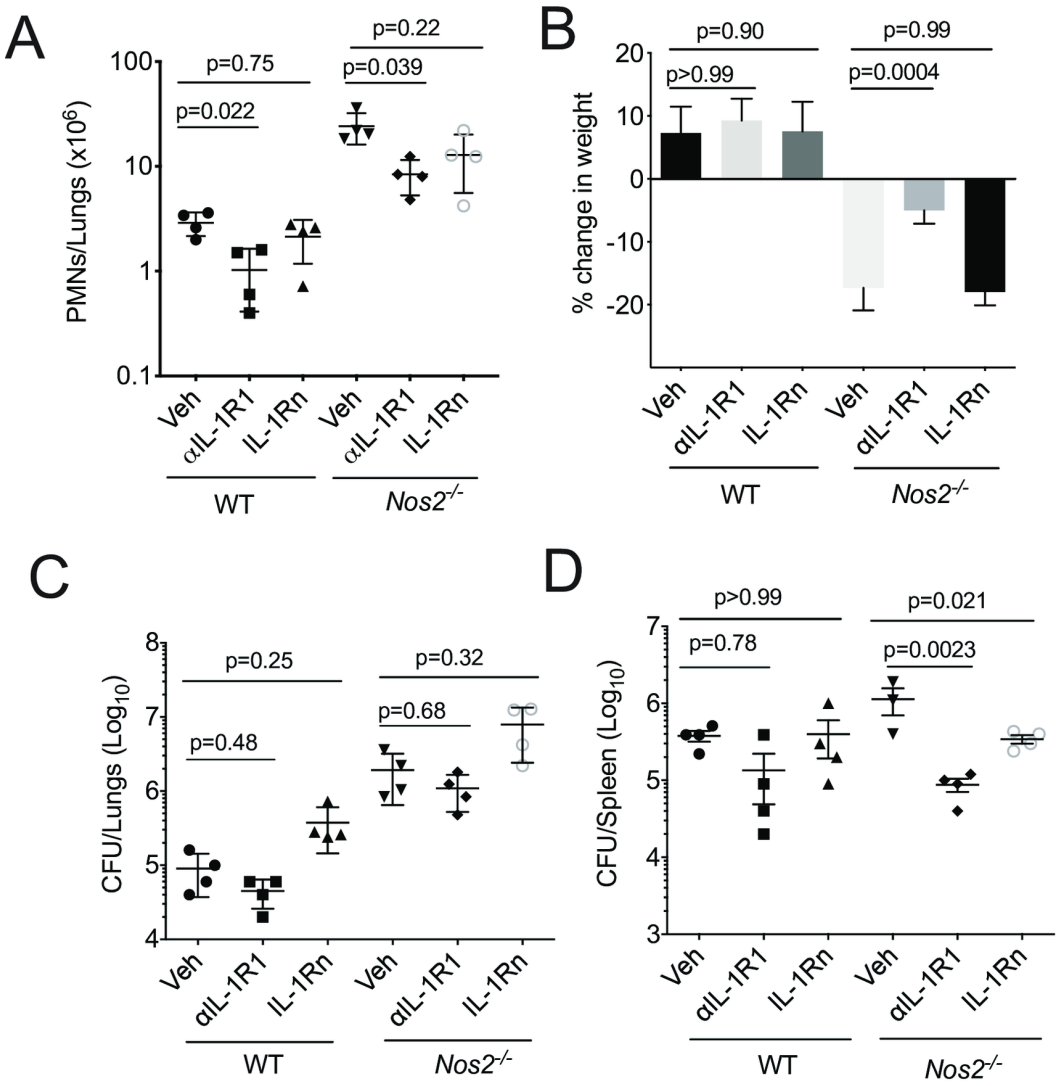

745

Figure 1. IL-1 inhibition in susceptible mice reduces inflammation with no effect on lung bacterial burden.

Wild type C57BL/6 and *Nos2*$^{-/-}$ mice were infected with Mtb Erdman for 2 weeks, and treated with anti-IL-1R1 (αIL-1R1) or IL-1R1-antagonist (IL-1Rn) for the subsequent 2 weeks. (A) Lung neutrophil (PMN) infiltration was quantified by flow cytometry; (B) Weight loss and (C) CFU in lung and (D) spleen are shown. Data shown (mean ± SD) are representative of two independent experiments. One-way ANOVA with Sidak's multiple comparisons-test was used. N=4 mice per treatment cohorts. (E) Histopathology analysis of a single lung lobe from WT or *Nos2-/-* mice was performed by Hematoxylin-eosin (H&E) staining.

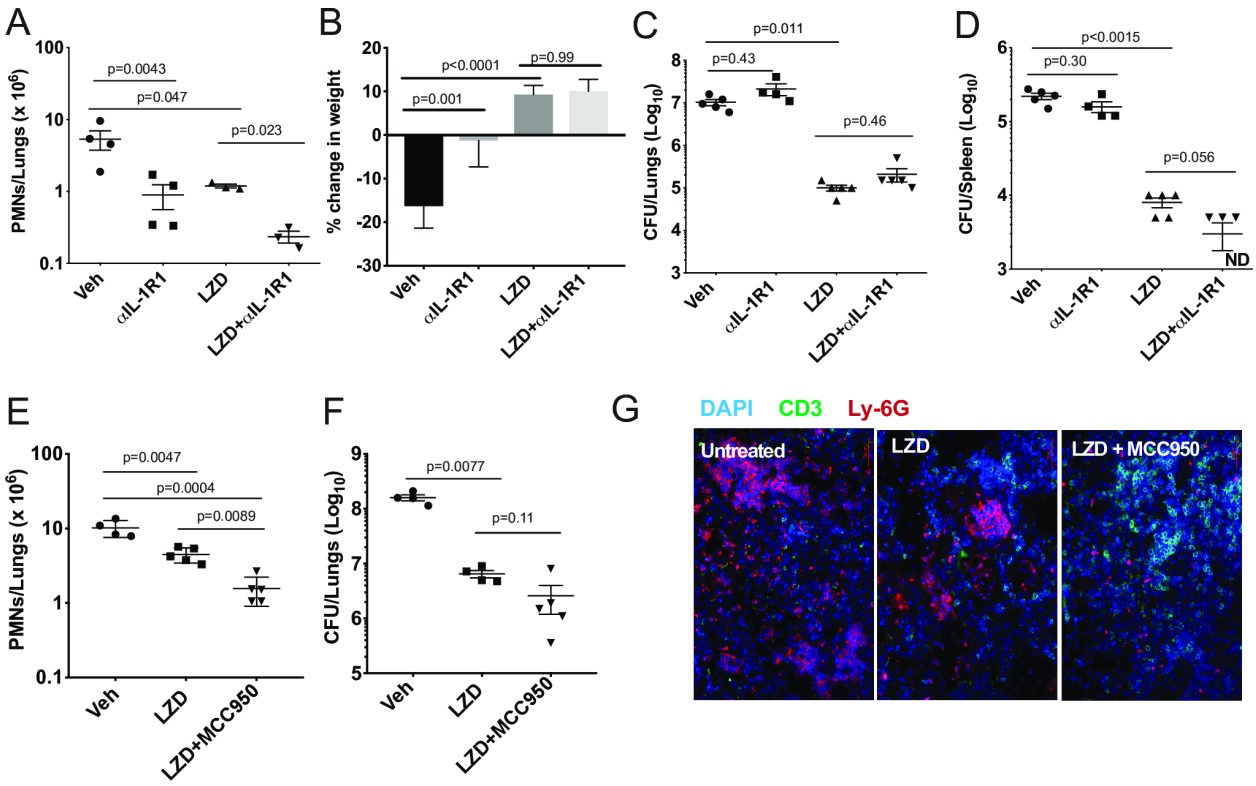

Figure 2. IL-1R1 blockade combined with Linezolid ameliorates TB disease.

(A-D) C3HeB/FeJ mice were infected with Mtb Erdman for 4 weeks and treated with linezolid (LZD) and/or anti-IL-1R1 (αIL-1R1) for the following 18 days. (A) Lung neutrophils were quantified by flow cytometry; (B) Percent change in body weight is shown and (C) Bacterial

burden in the lung and (D) spleen were quantified as CFU. Data shown (Mean ± SD) are representative of two independent experiments. Welch ANOVA with Dunnett's post-test was used to calculate statistical significance where each treatment group was compared to the vehicle as control group. N=3-5 mice per treatment group. (E-G) C3HeB/FeJ mice were infected with *M. tb* Erdman for 8 weeks and treated with linezolid (LZD) and/or an inhibitor of the NLRP3 inflammasome (MCC950) for the following 21 days. (E) Lung neutrophils were quantified by flow cytometry. (F) Bacterial burden in the lung was quantified by CFU. Data shown (Mean ± SD) are from one experiment. One-way ANOVA with Tukey's multiple comparison test was used to calculate the p-value. N=4-5 mice/group. (G) Representative immunofluorescence images of the lungs from different treatment groups. Cell nuclei stained with DAPI (blue), T-cells stained with anti-mouse CD3ε (green) and neutrophils stained with anti-mouse Ly-6G (red).

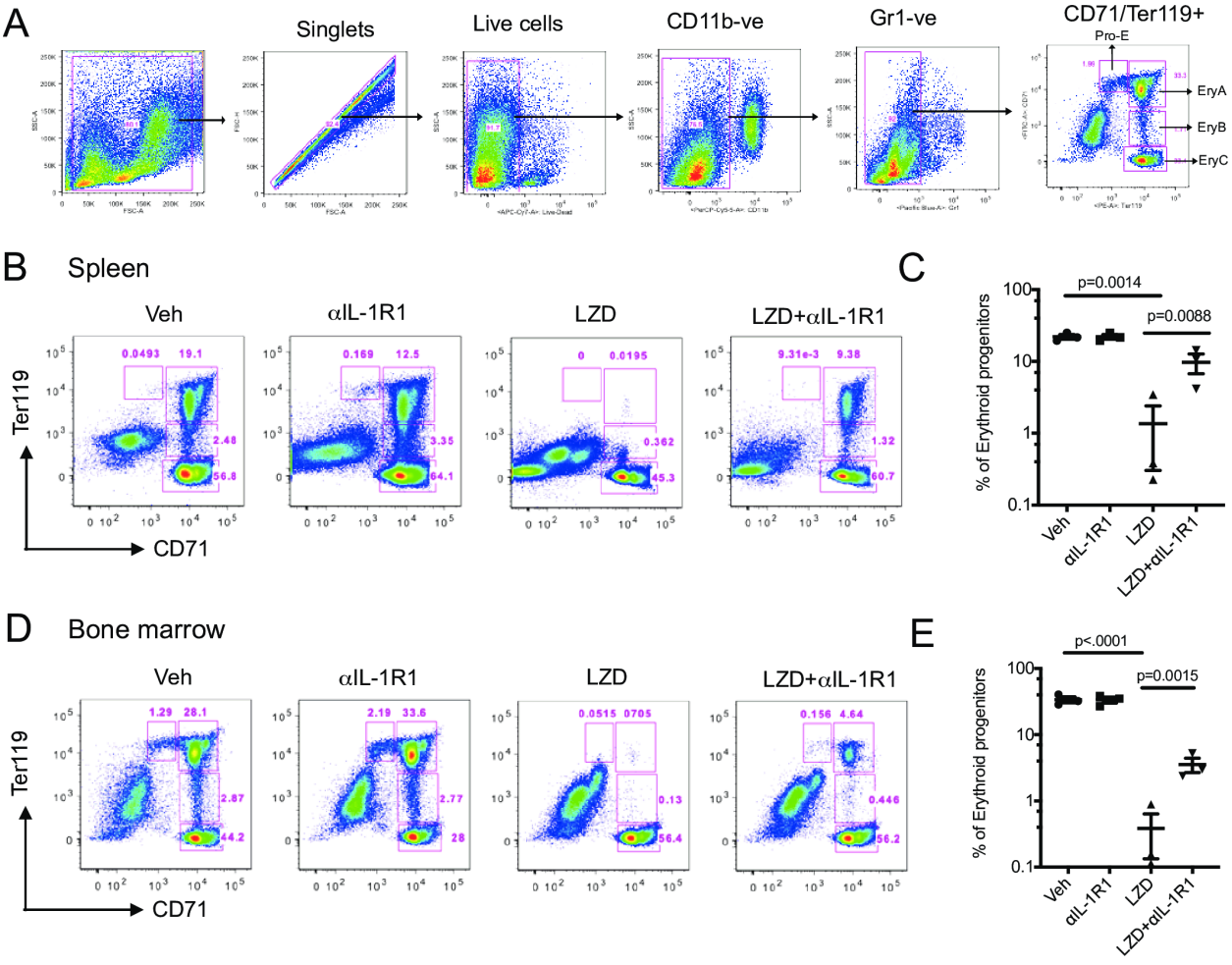

773 **Figure 3. Erythropoiesis associated with LZD treatment was partially relieved after IL-**
774 **1R1 blockade.**
775 C3HeB/FeJ mice were infected with Mtb Erdman for 4 weeks, and treated with LZD either alone
776 or in combination with anti-IL-1R1 antibody for the subsequent 18 days. (A) Gating strategy for
777 detecting erythroid progenitors is shown. Erythroid progenitors in the spleen (B-C) and bone
778 marrow (D-E) were quantified by flow cytometry as described in Materials and Methods.
779 Representative flow cytometry plots and percent changes in the early erythroid progenitors (Pro-
780 Ery, EryA, EryB) among different treatment groups are shown. Data shown (Mean ± SD) are
781 from two independent experiments. One-way ANOVA with Dunnett's post-test was applied to
782 calculate the p-value by comparing the mean of each group with that of LZD treated group.
783 N=3-5 mice per group.

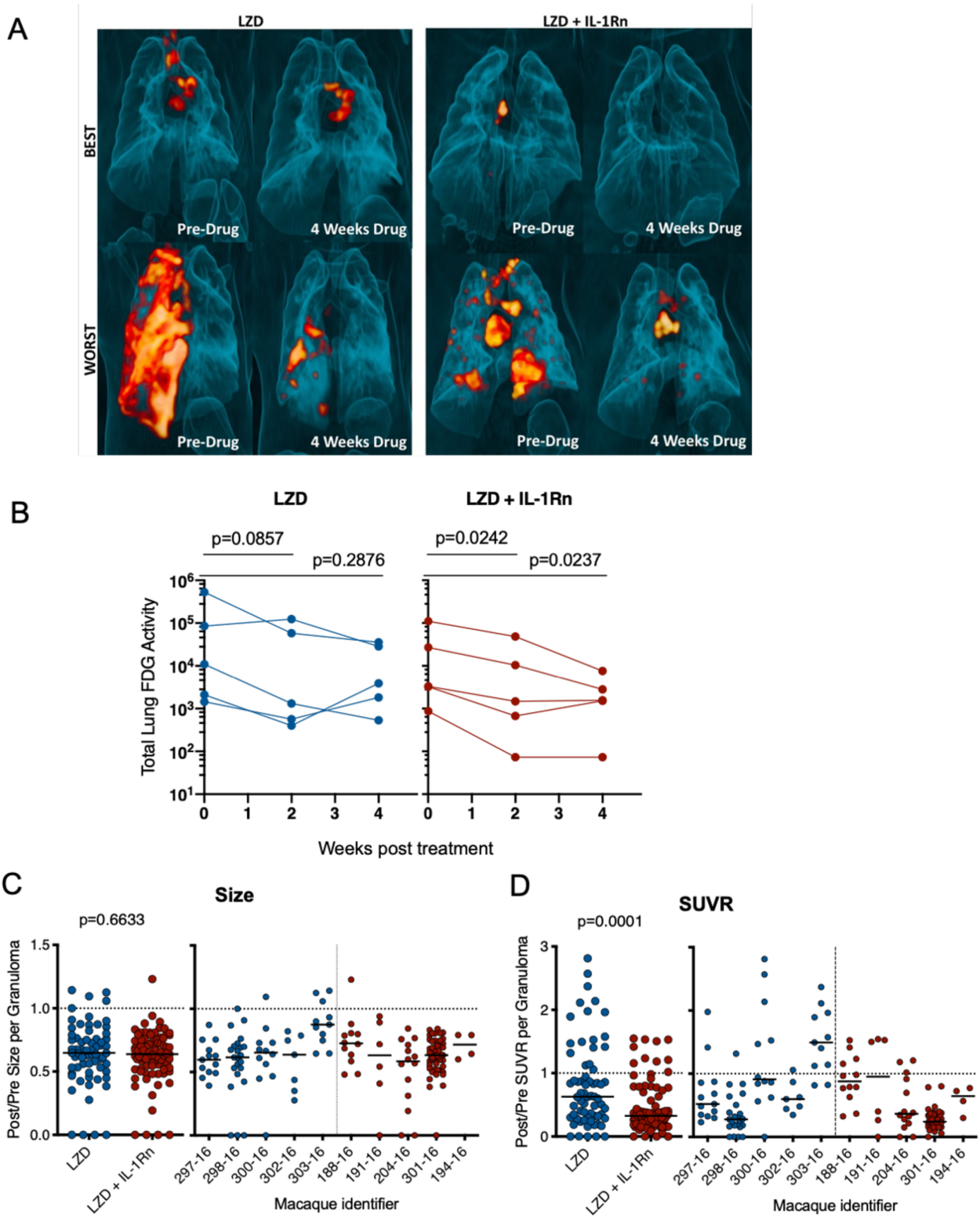

Figure 4. HDT reduces granuloma inflammation by PET/CT in macaques

Cynomolgus macaques were infected with *M. tb* Erdman for approximately 4 months (see Supplementary Table 1) and randomized to treatment with LZD or LZD+IL-1Rn for an additional 4 weeks. PET/CT scans were performed pre-treatment, 2 and 4 weeks post-treatment with 4 week scans as the last prior to necropsy. (A) 3-D renderings of PET/CT scans from pre-treatment and 4 weeks post-treatment are depicted, with “best” and “worst” of each group referring to TB disease prior to drug administration. (B) Total lung FDG activity of each macaque throughout treatment with LZD (left) or LZD+IL-1Rn (right). Two-way ANOVA with Dunnett’s adjusted p-values are reported. (C) Individual granulomas were identified pre-treatment and tracked post-treatment by PET/CT. Change in size (by CT) was determined for granulomas from each animal; the left graph is compiled granulomas from each animal in the indicated treatment groups while the right depicts individual animals. (D) Standard uptake value (SUVR) of ^{18}F-FDG was calculated for each granuloma, representing inflammation. Change in SUVR of all granulomas in each groupis depicted on the left, while change in SUVR of granulomas from each individual animal are on the right. For (C) and (D), each data point is representative of one granuloma and the bar represents the median. Mann-Whitney tests determined p values for (C) and (D), with $p<0.05$ considered significant.

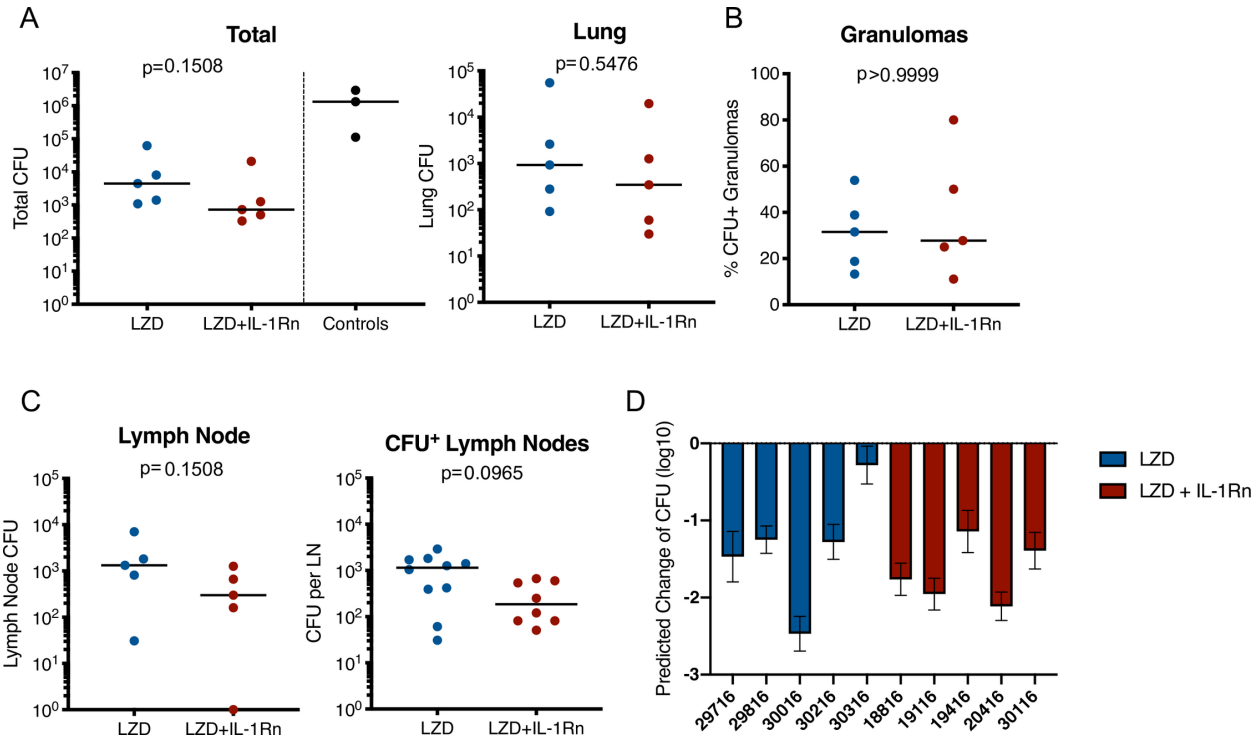

Figure 5. Addition of IL-1Rn does not enhance efficacy of LZD for bacterial killing

Bacterial burden is shown after 4 weeks of LZD (blue) or LZD+IL-1Rn (red) treatment. (A) Total thoracic (lung + lymph nodes) and lung CFU; each data point represents one macaque. Total thoracic CFU from 3 similarly infected untreated historical control macaques (black) are included as reference for untreated CFU at this time point, but excluded from statistical analysis. (B) The percent of all lung granulomas that were CFU+ per monkey. (C) CFU of all thoracic lymph nodes with data points representing CFU from one macaque. CFU+ lymph nodes show the CFU from each thoracic lymph node in any animal that was Mtb+. For (A) and (B), p values were determined by Mann-Whitney test. (C) PET/CT scans from pre-treatment were used to model predicted CFU prior to HDT initiation and compared to actual CFU determined at time of necropsy. The predicted change in CFU was determined by: Actual total thoracic CFU post-treatment– Predicted total thoracic CFU interval (predicted from pre-drug-treatment scan). Bars represent mean of prediction intervals and error whiskers represent the lower and upper bounds of the difference between final total CFU and predicted CFU prior to drug treatment.

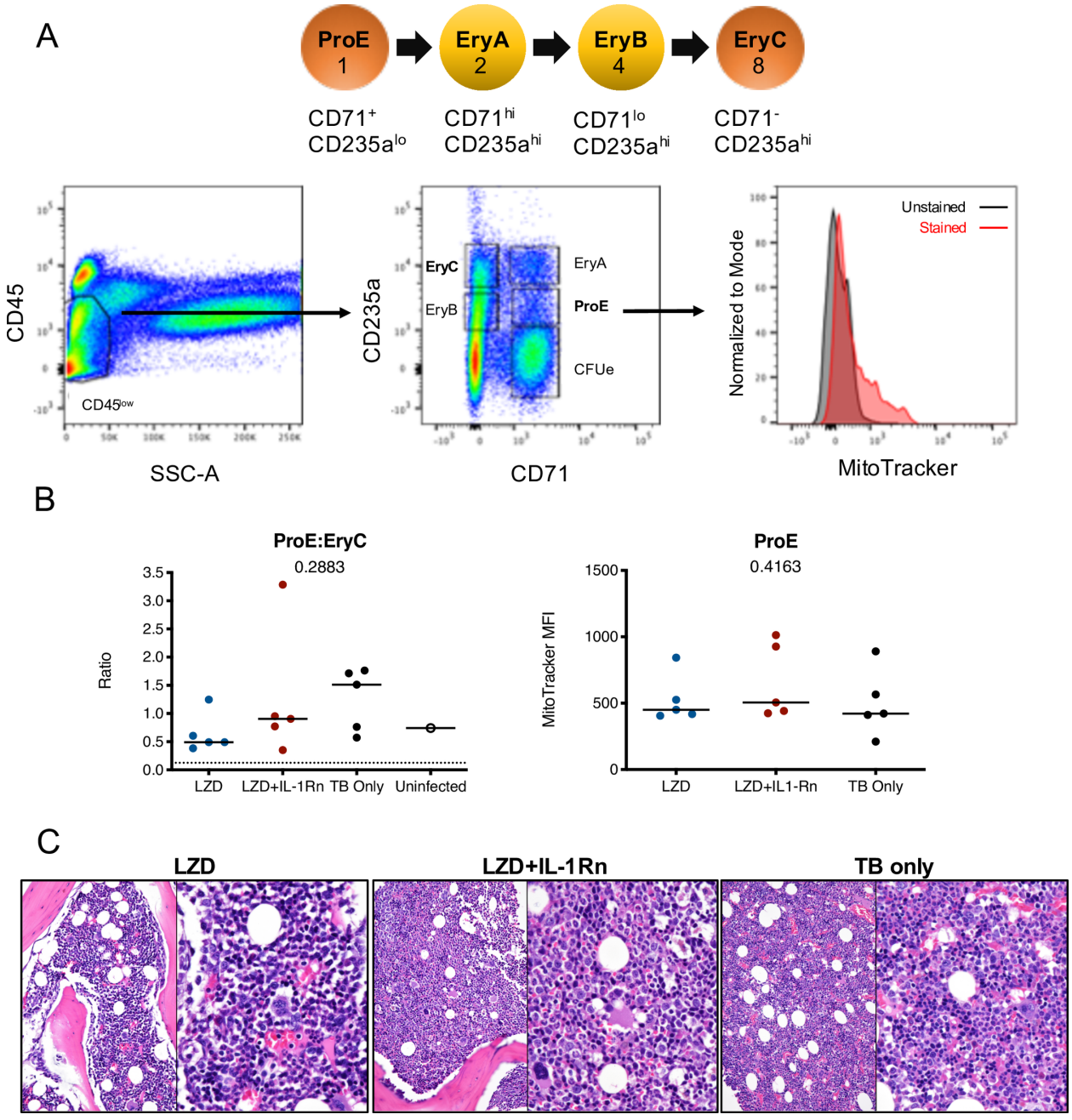

817

818 **Figure 6. Linezolid-associated bone marrow suppression was not observed in macaques**

819 Bone marrow was acquired from the sternum of all macaques at necropsy after 4 weeks LZD or

820 LZD+IL-1Rn. A portion was used for flow cytometric analysis of erythroid progenitor populations

821 and the rest for histopathology analysis. (A) A schematic of erythropoiesis indicating the stage

822 of differentiation and corresponding expression levels of phenotyping markers (CD235 and

823 CD71) and progenitor ratios (1:2:4:8). Included is the gating strategy to identify progenitor

824 populations and an example of MitoTracker staining. (B) The ProE:EryC ratio (left) of each
825 animal, including untreated TB only macaques (black) from other ongoing unpublished studies.
826 A single uninfected animal (open circle) is shown as reference, the dotted line indicates the
827 homeostatic ratio of 1:8. MitoTracker MFI (right) is shown for each macaque per treatment
828 group. Kruskal-Wallis test was performed to compare the three groups (excluding uninfected
829 macaque) and p values are shown in the graphs. (C) Representative H&E images from sternal
830 bone marrow acquired at necropsy, 20x (left) and 40x (right) are shown.

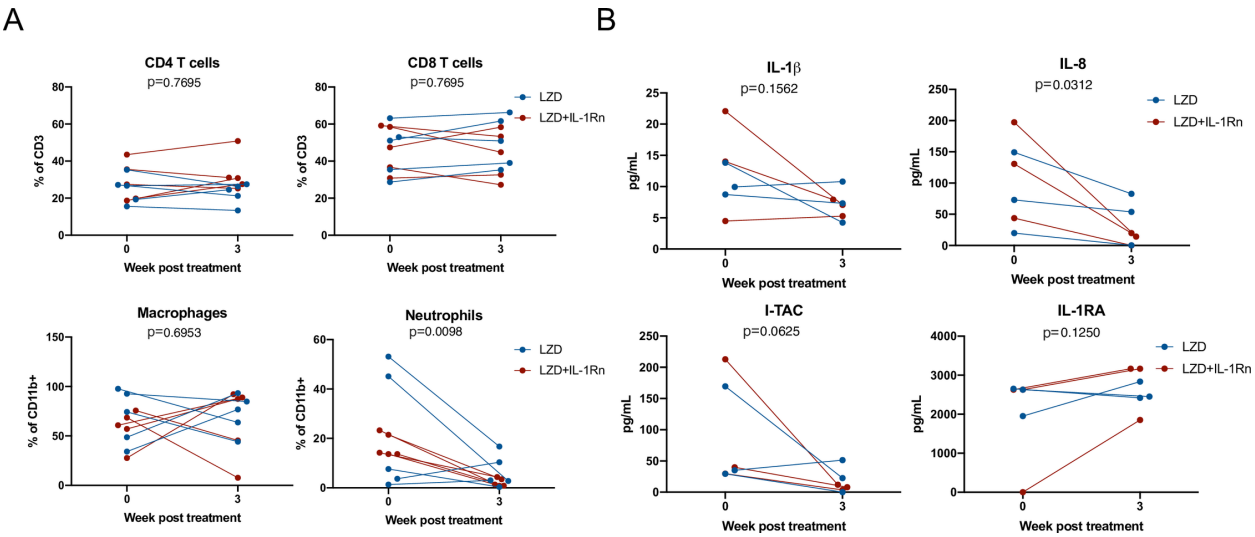

831

832 **Figure 7. HDT reduces inflammatory signatures in BAL**

833 Bronchoalveolar lavages (BAL) were acquired pre-treatment and 3 weeks post-treatment with
834 LZD (blue) or LZD+IL-1Rn (red). (A) Cells were analyzed by flow cytometry to determine
835 frequency changes in CD4 T cells (CD3+CD4+), CD8 T cells (CD3+CD8+), macrophages
836 (CD11b+CD206+) and neutrophils (CD11b+Calprotectin+). Wilcoxon signed rank test was
837 performed to determine differences before and after drug treatment, regardless of group (LZD
838 and LZD+IL-1Rn combined). (B) BAL fluid was concentrated 10X and assessed by multiplex
839 assay for changes in inflammatory cytokines and chemokines for a random subset of samples
840 (n=3 per treatment group). Wilcoxon signed rank test was performed to determine differences
841 before and after drug treatment, regardless of group (LZD and LZD+IL-1Rn combined).

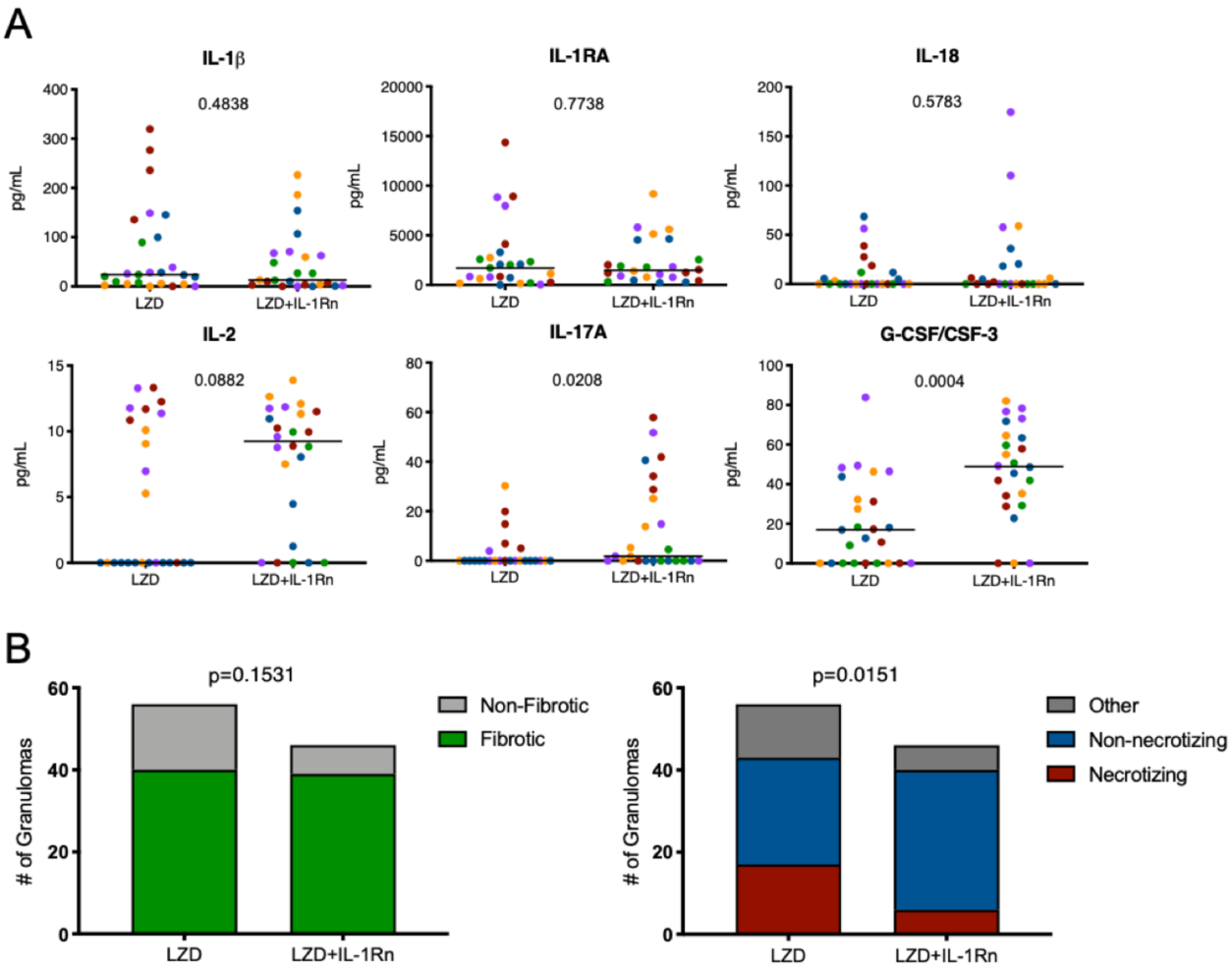

Treatment	% Fibrotic	% Non-necrotizing	% Necrotizing
LZD	71.43	46.43	30.36
LZD+IL1-Rn	84.78	73.91	13.04

Figure 8. Inflammation modulation by HDT influences granuloma resolution

Randomly selected granulomas (n=5 per macaque, n=25 per treatment group) were subjected to multiplex analysis to determine differences between treatment groups (colors indicate lesions from a single animal). p values shown determined by Mann-Whitney test. (B) Granulomas from LZD (n=57) and LZD+IL-1Rn (n=45) were examined by a pathologist (EK) and categorized. We compared fibrotic (green) vs non-fibrotic (light gray) (left) and necrotizing (red) vs non-

849 necrotizing (blue) granuloma frequencies. Frequencies represent the percentage of all

850 granulomas within treatment groups. Fisher's exact test p-values are reported.

851

852 ## Supporting information

853 **Supplementary Table 1. List of macaques for study and PET/hot values.**

854 Provided are details regarding macaques utilized for this study. DPI = days post infection.

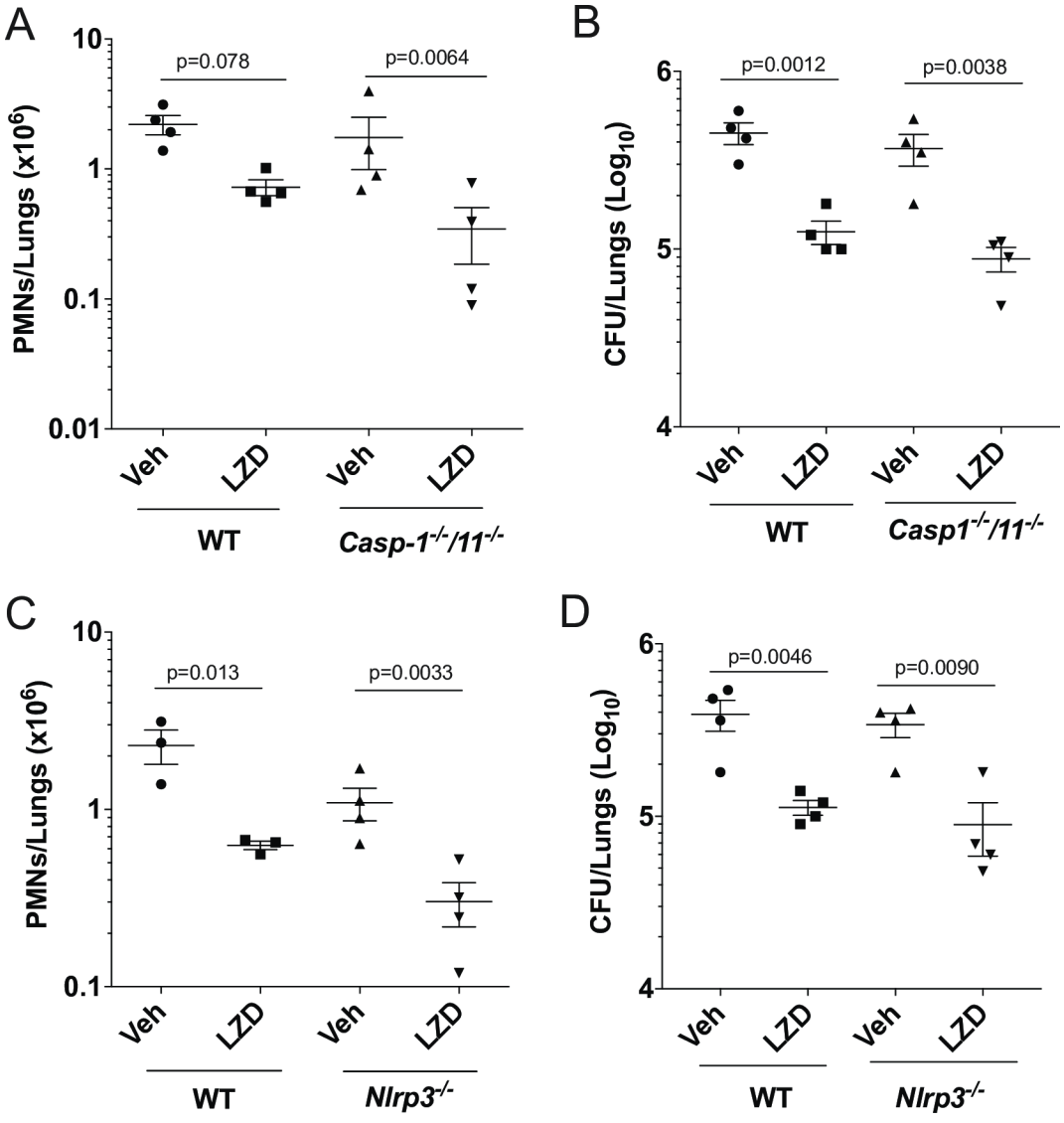

855

856 **S1 Fig. Inhibiting inflammasome signaling does not interfere with LZD efficacy.**

857 (A) Wild type C57BL/6 and *Caspase-1/11*$^{-/-}$ mice were infected with *M. tb* Erdman for 2 weeks,
858 and treated with linezolid for the subsequent 2 weeks. (A) Lung neutrophil (PMN) infiltration was
859 quantified by flow cytometry. (B) CFU in the lung are shown. Data shown (Mean ± SD) are
860 representative of two independent experiments. (C) WT and *Nlrp3*$^{-/-}$ mice were infected with *M.*
861 *tb* Erdman for 2 weeks and treated with linezolid for the following two weeks. (C) Lung
862 neutrophils were quantified by flow cytometry. (D) Bacterial burden in the lung were quantified
863 as CFU. Data shown (Mean ± SD) are from one experiment. One-way ANOVA with Sidak's
864 multiple comparison test was used to calculate the indicated p-values. N=3-5 mice used for
865 each treatment group.
866

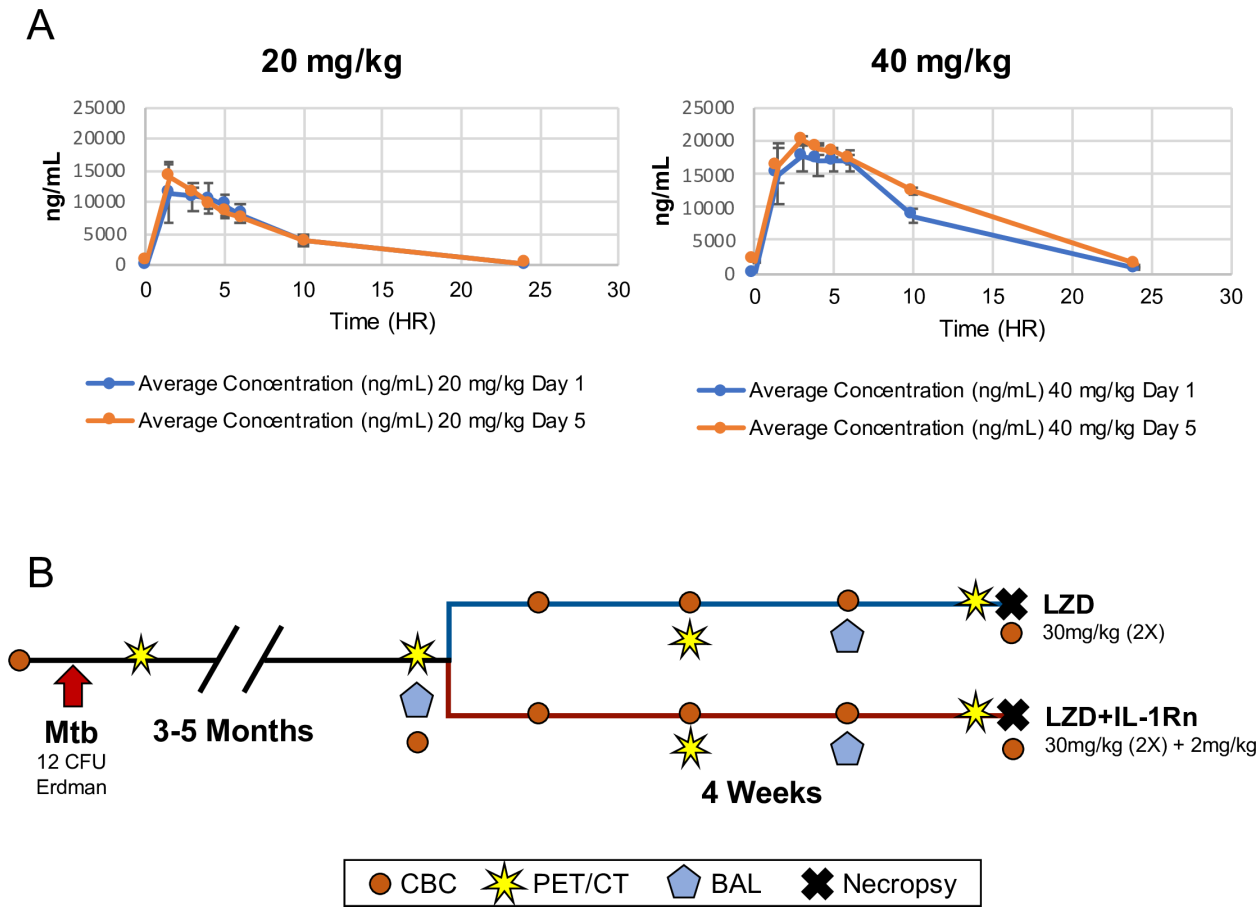

867

868 **S2 Fig. Linezolid pharmacokinetic analyses and Experimental plan for HDT in macaques**

869 (A) Plasma concentration time profiles of cynomolgus macaques receiving 20mg/kg or 40mg/kg
870 linezolid. Average plasma concentrations were plotted on Day 1 and Day 5 post-dose (n=3) (B)
871 Experimental timeline of macaque study.

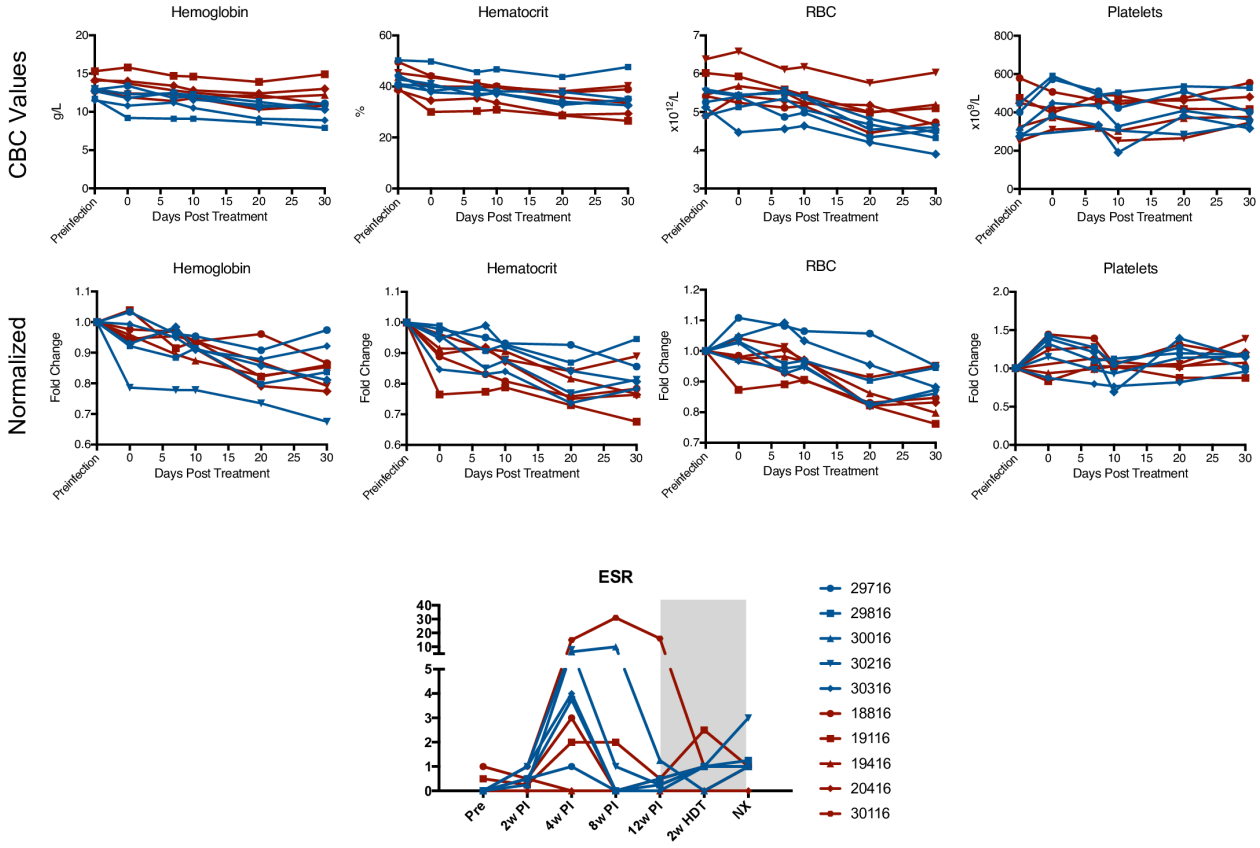

872

873 **S3 Fig. Complete blood counts and erythrocyte sedimentation rate for macaques**
874 **undergoing HDT**

875 Complete blood counts (CBCs) were taken through the study to assess anemia caused by
876 linezolid or Mtb infection. The CBC values (top) show true values for each macaque in LZD
877 (blue) or LZD+IL-1Rn (red) treatment groups. Due to variability in animal size and age, we
878 normalized CBC values to the preinfection time point for each animal (middle graphs). These
879 data indicate the relative change over the course of HDT. ESR (bottom) is a non-specific
880 measure of inflammation, LZD (blue) and LZD+IL-1Rn (red) treated macaques are depicted.

881